

# Structural and thermodynamic insights into the binding mode of five novel inhibitors of lumazine synthase from *Mycobacterium tuberculosis*

Ekaterina Morgunova<sup>1</sup>, Boris Illarionov<sup>2</sup>, Thota Sambaiah<sup>3</sup>, Ilka Haase<sup>2</sup>, Adelbert Bacher<sup>2</sup>, Mark Cushman<sup>3</sup>, Markus Fischer<sup>2</sup> and Rudolf Ladenstein<sup>1</sup>

<sup>1</sup> Karolinska Institutet, NOVUM, Centre for Structural Biochemistry, Huddinge, Sweden

<sup>2</sup> Lehrstuhl für Organische Chemie und Biochemie, Technische Universität München, Garching, Germany

<sup>3</sup> Department of Medicinal Chemistry and Molecular Pharmacology, and the Purdue Cancer Center, School of Pharmacy and Pharmaceutical Sciences, Purdue University, West Lafayette, IN, USA

## Keywords

crystal structure; inhibition; lumazine synthase; *Mycobacterium tuberculosis*

## Correspondence

E. Morgunova, Karolinska Institutet, Department of Bioscience and Nutrition, Centre for Structural Biochemistry, S-14157 Huddinge, Sweden  
Fax: +46 8 6089290  
Tel: +46 8 608177  
E-mail: katja.morgunova@biosci.ki.se

(Received 26 June 2006, revised 23 August 2006, accepted 23 August 2006)

doi:10.1111/j.1742-4658.2006.05481.x

Recently published genomic investigations of the human pathogen *Mycobacterium tuberculosis* have revealed that genes coding the proteins involved in riboflavin biosynthesis are essential for the growth of the organism. Because the enzymes involved in cofactor biosynthesis pathways are not present in humans, they appear to be promising candidates for the development of therapeutic drugs. The substituted purinetrione compounds have demonstrated high affinity and specificity to lumazine synthase, which catalyzes the penultimate step of riboflavin biosynthesis in bacteria and plants. The structure of *M. tuberculosis* lumazine synthase in complex with five different inhibitor compounds is presented, together with studies of the binding reactions by isothermal titration calorimetry. The inhibitors showed the association constants in the micromolar range. The analysis of the structures demonstrated the specific features of the binding of different inhibitors. The comparison of the structures and binding modes of five different inhibitors allows us to propose the ribityl-purinetrione compounds with C4–C5 alkylphosphate chains as most promising leads for further development of therapeutic drugs against *M. tuberculosis*.

Vitamin B<sub>2</sub>, commonly called riboflavin, is one of eight water-soluble B vitamins. Like its close relative, vitamin B<sub>1</sub> (thiamine), riboflavin plays a crucial role in certain metabolic reactions, for example, in the final metabolic conversion of monosaccharides, where reduction-equivalents and chemical energy in the form of ATP are produced via the Embden–Meyerhoff pathway. Higher animals, including humans, are dependent on riboflavin uptake through their diet. However, most of the known microorganisms and a number of pathogenic enterobacteria are absolutely

dependent on the endogenous synthesis of riboflavin because they are unable to take up the vitamin from the environment. Because the enzymes involved in riboflavin biosynthesis pathways are not present in the human or animal host, they are promising candidates for the inhibition of bacterial growth.

*Mycobacterium tuberculosis* is one of the human pathogens responsible for causing eight million cases of new infections and two million human deaths every year in both developing and industrialized countries [1]. Treatment of the active forms of the disease has

## Abbreviations

ITC, isothermal titration calorimetry; JC33, [4-(6-chloro-2,4-dioxo-1,2,3,4-tetrahydropyrimidine-5-yl)butyl] 1-phosphate; LS, lumazine synthase; MbtLS, *Mycobacterium tuberculosis* lumazine synthase; MPD, (+/–)-2-methyl-2,4-pentandiol; RS, riboflavin synthase; TS13, 1,3,7-trihydro-9-D-ribityl-2,4,8-purinetrione; TS50, 5-(1,3,7-trihydro-9-D-ribityl-2,4,8-purinetrione-7-yl)pentane 1-phosphate; TS68, 6-(1,3,7-trihydro-9-D-ribityl-2,4,8-purinetrione-7-yl)hexane 1-phosphate; TS51, 5-(1,3,7-trihydro-9-D-ribityl-2,4,8-purinetrione-7-yl)1,1-difluoropentane 1-phosphate.

become increasingly difficult because of the growing antibiotic resistance of *M. tuberculosis*. The elucidation of the complete genomes of *M. tuberculosis* and the related *Mycobacterium leprae* has provided powerful tools for the development of novel drugs that are urgently required [2–4]. Both *M. tuberculosis* and *M. leprae* comprise complete sets of genes required for the biosynthesis of riboflavin (vitamin B<sub>2</sub>). As the genome of *M. leprae* has undergone a dramatic process of gene fragmentation, the fact that all riboflavin biosynthesis genes were retained in apparently functional form indicates that the biosynthetic pathway is of vital importance for the intracellular lifestyle of the pathogen. By extrapolation of this argument, it appears likely that the riboflavin pathway genes are also essential for *M. tuberculosis*.

The biosynthesis of riboflavin has been studied extensively over recent years. Two enzymes, lumazine synthase (EC 2.5.1.9; LS) and riboflavin synthase (RS), catalyzing the penultimate and the last step of riboflavin biosynthesis, respectively, are the main targets of our interest. It has been shown that in *Bacillus subtilis*, these two enzymes form a complex comprised of an inner core consisting of three  $\alpha$ -subunits (RS) encapsulated by an icosahedral shell containing 60  $\beta$ -subunits (LS) [5,6]. The  $\beta$ -subunits catalyze the turnover of 3,4-dihydroxy-2-butanone-4-phosphate (**2**) and 5-amino-6-ribitylamino-2,4(1*H*,3*H*)-pyrimidinedione (**1**) to 6,7-dimethyl-8-(*D*-ribityl)-lumazine (**3**), whereas the  $\alpha$ -subunits catalyze the formation of one riboflavin molecule from two molecules of (**3**), respectively (Fig. 1). The isolation and purification of LSs from

different organisms has revealed the pentameric nature of this enzyme, which can be found in two different oligomeric states. In *B. subtilis*, *Aquifex aeolicus* and *Spinacia oleracea*, the protein exists as an icosahedral capsid formed from 60 identical subunits (12 pentamers) [7–9]. LSs from *Saccharomyces cerevisiae*, *Schizosaccharomyces pombe*, *Brucella abortus* and *Magnaporthe grisea* are homopentameric enzymes [9–12]. Recently, we have solved the structure of LS from *M. tuberculosis*, which has shown the homopentameric state as well [13]. The LS monomer shows some folding similarity to bacterial flavodoxins [14] and is constructed from a central four-stranded  $\beta$ -sheet flanked on both sides by two and three  $\alpha$ -helices, respectively.

In spite of the fact that riboflavin biosynthesis was studied for several decades, the chemical nature of the second LS substrate, the four-carbon precursor of the pyrazine ring, remained unknown for a long time. The elucidation of the structure of this compound by Volk and Bacher in 1991 [15] allowed detailed studies of lumazine synthase catalysis. In order to investigate the catalytic mechanism of the formation of 6,7-dimethyl-8-(*D*-ribityl)-lumazine, Cushman and coworkers have designed and synthesized several series of inhibitors that mimic the substrate, the intermediates and the product of the reaction [16–22] catalysed by LS. The first detailed description of the active site of LS was provided by the X-ray structure of *B. subtilis* LS in complex with the substrate analogue 5-nitro-6-*D*-ribitylamino-2,4(1*H*,3*H*) pyrimidinedione [23]. It has been shown that the lumazine synthase active site is located at the interface of two neighbouring subunits and, furthermore,

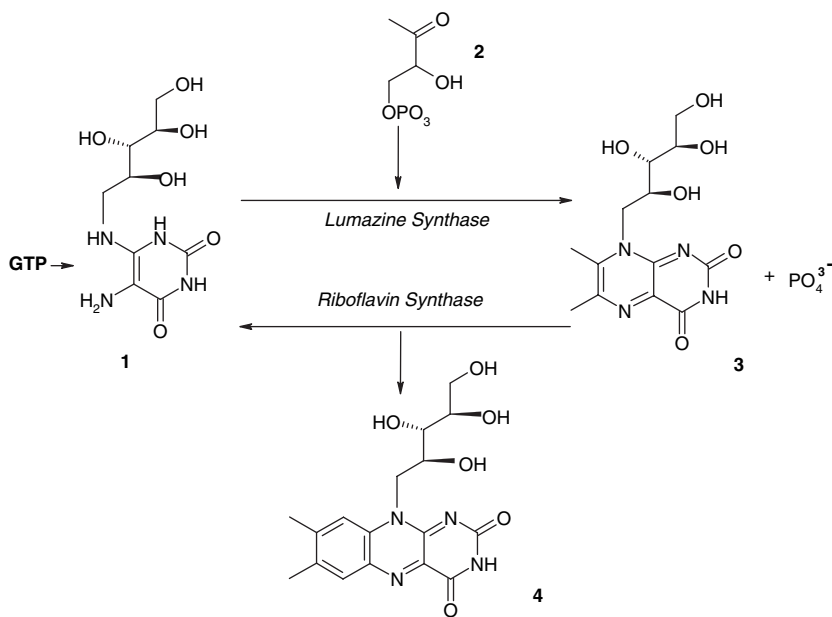


**Fig. 1.** Terminal reactions catalyzed by lumazine synthase and riboflavin synthase in the pathway of riboflavin biosynthesis. **1**, 5-Amino-6-ribitylamino-2,4(1*H*,3*H*)-pyrimidinedione; **2**, 3,4-dihydroxy-2-butanone-4-phosphate; **3**, 6,7-dimethyl-8-ribityl-lumazine; **4**, riboflavin.

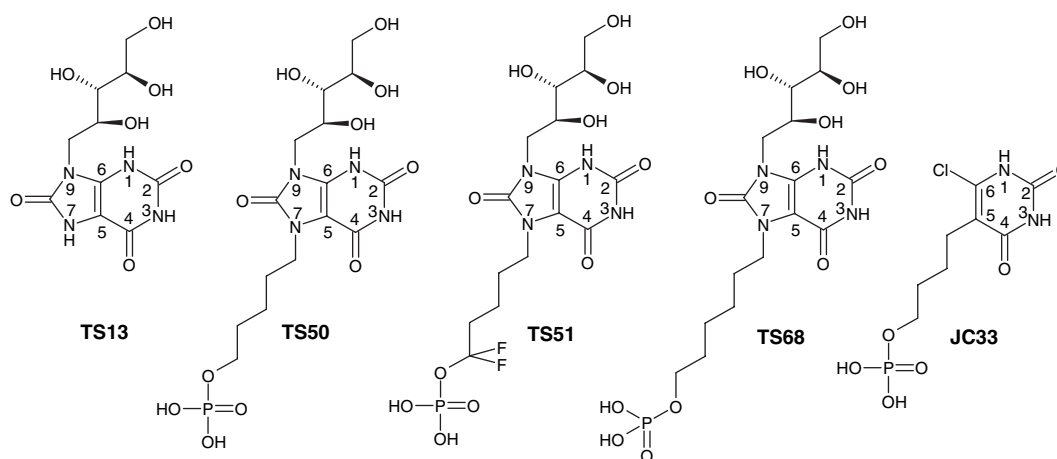


**Fig. 2.** Inhibitors of lumazine synthase from *M. tuberculosis*: 1,3,7-trihydro-9-D-ribyl-2,4,8-purinetrione (TS13), 5-(1,3,7-trihydro-9-D-ribyl-2,4,8-purinetrione-7-yl)pentane 1-phosphate (TS50), 6-(1,3,7-trihydro-9-D-ribyl-2,4,8-purinetrione-7-yl)hexane 1-phosphate (TS68), 5-(1,3,7-trihydro-9-D-ribyl-2,4,8-purinetrione-7-yl) 1,1-difluoropentane 1-phosphate (TS51), [4-(6-chloro-2,4-dioxo-1,2,3,4-tetrahydropyrimidin-5-yl)butyl]1-phosphate (JC33).

that it is built by highly conserved hydrophobic and positively charged residues from both subunits.

Lumazine synthase inhibitors can be considered as potential lead compounds for the design of therapeutically useful antibiotics. Recently, a new series of compounds based on the purinetrione aromatic system was designed [22,24]. Somewhat later it was found that those compounds demonstrated the highest binding affinity and specificity to LS from *M. tuberculosis* in comparison with the LSs from other bacteria. Two structures of *M. tuberculosis* LS in complex with two ribityl-purinetrione compounds bearing an alkyl phosphate group were solved and published recently by our group [13]. In order to provide structural information for the design of optimized LS inhibitors, we have undertaken the structure determination of *M. tuberculosis* LS complexes with four differently modified purinetrione compounds. Binding constants and other thermodynamic binding parameters were determined by isothermal titration calorimetry (ITC) experiments. In this paper, we also present the structure of a complex of *M. tuberculosis*, MbtLS, with [4-(6-chloro-2,4-dioxo-1,2,3,4-tetrahydropyrimidine-5-yl)butyl] 1-phosphate, which is the first LS/RS inhibitor lacking the ribityl chain. In addition, ITC results for its binding are presented.

## Results and Discussion

### Structure determination and quality of the refined models

All structures presented in our paper were determined by molecular replacement. The cross-rotation and

translation searches performed with AMORE in the case of the MbtLS/TS50 complex yielded a single dominant solution. The same was true for the complexes of MbtLS with TS51 and JC33, which were solved in MOLREP. Solutions for two pentamers with good crystal packing were obtained for the data sets of MbtLS/TS13 and MbtLS/TS68. The structures were refined to crystallographic R-factor values of 24.5% ( $R_{\text{free}} = 32.7\%$ ) (MbtLS/TS13), 18.2% ( $R_{\text{free}} = 22\%$ ) (MbtLS/TS50), 17.5% ( $R_{\text{free}} = 21.9\%$ ) (MbtLS/TS51), 25.8% ( $R_{\text{free}} = 32.6\%$ ) (MbtLS/TS68) and 14.6% ( $R_{\text{free}} = 21.4\%$ ) (MbtLS/JC33), and with good stereochemistry (Table 1).

The main chain atoms were well defined in all structures, including the structure of the complexes MbtLS/TS13 and MbtLS/TS68, with the exception of 13 N-terminal residues, which remained untraceable in all subunits of all structures. The residues His28 (A-subunit), Asp50 (C-subunit) and Ala15 (F-subunit) in the MbtLS/TS13 complex and residues Ala15 (A-, D- and I-subunits) in MbtLS/TS68 had to be fitted to a very poor density. However, they were found in additionally allowed regions in the Ramachandran plot at the end of refinement. All ligands were well defined in the electron density map.

The structure of the pentameric MbtLS has been described in detail in [13]. In brief, MbtLS, as well as all other known LS orthologues, belong to the family of  $\alpha/\beta$  proteins with an  $\alpha/\beta/\alpha$  sandwich topology (Fig. 3). The core of a subunit consists of a central four-stranded parallel  $\beta$ -sheet flanked by two  $\alpha$ -helices on one side and three  $\alpha$ -helices on the other side. Five equivalent subunits form a pentamer of the

**Table 1.** Data collection and refinement statistics.

Data collection	MbtLS/TS13	MbtLS/TS50	MbtLS/TS51	MbtLS/TS68	MbtLS/JC33
<b>Cell constants (Å, °)</b>					
a	78.1	131.4	131.4	79.9	131.6
b	78.4	80.8	81.2	79.9	82.3
c	88.8	85.9	85.8	88.3	86.4
α	64.4	90	90	64.3	90
β	64.7	90	90	64.4	90
γ	65.0	120.2	120.2	62.8	120.3
<b>Space group</b>	P1	C2	C2	P1	C2
<b>Z*</b>	10	5	5	10	5
<b>Resolution limit (Å)</b>					
[highest shell]	[2.71–2.65]	[1.64–1.60]	[1.94–1.90]	[2.86–2.80]	[2.02–2.00]
Number of observed reflections	23 9902	55 2894	41 1396	25 4050	52 8273
Number of unique reflections	59 532	10 3691	58 728	77 471	51 716
<b>Completeness overall (%)</b>					
	89.1 (85.7)	85.8 (80.3)	95.5 (89.0)	84.0 (80.9)	96.5 (71.7)
<b>Overall I/σ</b>					
	4.4 (1.25)	2.4 (1.37)	13.5 (2.33)	4.0 (1.24)	8.2 (1.62)
<b>R<sub>sym</sub> overall (%)<sup>a</sup></b>					
	14.9 (47.5)	3.8 (55.5)	5.4 (4.36)	11.6 (57.3)	11.2 (52.0)
<b>Wilson plot (Å<sup>2</sup>)</b>					
	67.8	22.4	25.1	70.4	31.8
<b>Refinement</b>					
Resolution range (Å)	12.92–2.65	15.5–1.6	19.92–1.9	12.5–2.8	14.9–2.5
Non hydrogen protein atoms	10 660	5302	5270	10 598	5284
Non hydrogen inhibitor atoms	210 (21 × 10)	155 (31 × 5)	160 (32 × 5)	320 (32 × 10)	90 (18 × 5)
<b>Solvent molecules</b>					
	694	705	558	530	634
<b>Solvent ions</b>					
	*22*	*13*	*17*	*17*	*36*
<b>R<sub>cryst</sub> overall (%)<sup>b</sup></b>					
	24.5	18.2	17.5	25.8	14.5
<b>R<sub>free</sub> (%)<sup>c</sup></b>					
	32.7	22.0	21.9	32.6	21.4
<b>Ramachandran plot</b>					
Most favourable regions (%)	93.9	93.4	95.0	92.9	91.8
Allowed regions (%)	5.9	6.6	5.0	7.0	8.2
Disallowed regions (%)	0.2	0.0	0.0	0.2	0.0
<b>r.m.s. standard deviation</b>					
Bond lengths (Å)	0.007	0.010	0.008	0.007	0.011
Bond angles (°)	1.180	1.650	1.415	1.280	1.413
Average B-factors/SD (Å <sup>2</sup> )	35.2	24.8	30.6	32.6	25.4

\*Z is a number of the protein molecules per asymmetric unit. The values for the highest resolution shells are represented in square parenthesis. The amounts of the ions included to the refinement are presented in between asterisks. <sup>a</sup> $R_{sym} = \sum_i |I_i - \langle I_i \rangle| / \sum_i \langle I_i \rangle$ , where  $I_i$  is scaled intensity of the  $i$ th observation and  $\langle I_i \rangle$  is the mean intensity for that reflection. <sup>b</sup> $R_{crys} = \sum_{hkl} ||F_{obs}| - |F_{calc}|| / \sum_{hkl} |F_{obs}|$ . <sup>c</sup> $R_{free}$  is the cross-validation R factor computed for the test set of 5% of unique reflections.

active enzyme. The central pentameric channel is formed by five  $\alpha$ -helices arranged in the form of a super-helix around the five-fold axis. In four of the five structures presented in our work, the channel is occupied by a 2-methyl-2,4-pentanediol (MPD) molecule, whereas the channel of LS from *A. aeolicus* is filled with water molecules and/or a phosphate ion [8,25] and the channel of LS from *M. grisea* is filled with a sulfate ion [9]. The bound MPD molecule is surrounded by the side-chain atoms of Gln99 from one or two subunits. Nitrogen atom Gln99N<sup>e2</sup> forms a hydrogen bond with MPDO4 (distance 3 Å), oxygen Gln99O<sup>e1</sup> makes two interactions with MPDO2 and MPDO4 atoms (distances 3.8 and 3.5 Å, respectively). The structural superposition of the pentamer-

ic complexes with different inhibitors showed a highly conserved arrangement of the pentamers, independent of the nature of the inhibitor. Lumazine 3 (Fig. 1) is formed in the active sites located at the interfaces between adjacent subunits in the pentamer. Each active site contains a cluster of highly conserved amino acid residues and is composed in part by the residues donated from the closely related neighbouring monomer, i.e. the residues 26–28 from loop connecting  $\beta$ 2 and  $\alpha$ 1, residues 58–61 from loop connecting  $\beta$ 3 and  $\alpha$  and residues 81–87 from loop connecting  $\beta$ 4 and  $\alpha$ 3 from one subunit and the residues 114 and 128–141 from  $\beta$ 5 and  $\alpha$ 4- and  $\alpha$ 5-helices from the neighbouring subunit (Fig. 3) [13].

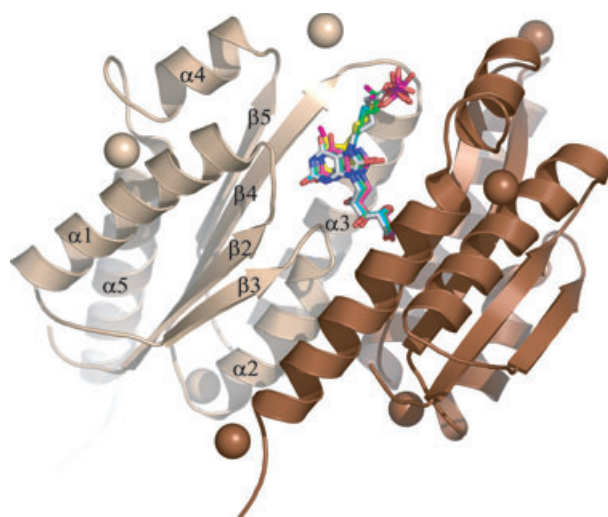


**Fig. 3.** The active sites of lumazine synthase are located at the interface of two neighbouring subunits, coloured beige and brown. Spheres indicate the potassium atoms belonging to the respective subunit. Secondary structure elements are indicated (spiral =  $\alpha$ -helix; arrow =  $\beta$ -strand). The inhibitors TS13, TS50, TS68, TS51 and JC33 are superimposed in the active site. The figure was generated with PYMOL [38].

### Crystal packing

The packing mode of two pentamers sharing a common five-fold axis in space group P1 (complexes with TS13 and TS68) mimics the packing of two pentamers from adjacent asymmetric units connected by a two-fold crystallographic axis as observed in the structures refined in space group C2 (Fig. 4). This kind of

contact is reminiscent of a similar packing interaction that has been observed between pentamers in crystals of *S. cerevisiae* LS belonging to space group P4<sub>1</sub>2<sub>1</sub>2, with one pentamer in the asymmetric unit [12]. However, LSs from *B. abortus*, *S. pombe* and *M. grisea* demonstrated a different, so-called ‘head-to-head’, pentameric contact in their crystals, although those three enzymes were crystallized in different space groups. In comparison with the interfaces of MbtLS and *S. cerevisiae* LS, the ‘head-to-head’ interface is formed by opposite surfaces of the pentameric disk. This assembly of two pentamers to form a decamer is claimed to be stable in solution for *Brucella* spp. LS [26].

Both pentamers in MbtLS connected by a two-fold crystallographic axis in case of space group C2 crystals or by a local two-fold in space group P1 bury an area of almost 8225 Å<sup>2</sup> in the interface between two disk-like pentamers (Fig. 4), whereas in *S. cerevisiae* LS the respective buried interface area is only 1271.5 Å<sup>2</sup>. Nineteen residues from each of 10 MbtLS subunits involved in the contacts sum up to totally 190 residues in the decamer interface. A total of 15 potassium ions are also found in the mentioned area (Figs 4 and 5). In comparison, there are only six residues per monomer involved in the symmetrical contacts in *S. cerevisiae* LS. Furthermore, no ions were observed in the contact surface. Every subunit of one MbtLS pentamer forms nine contacts with three adjacent subunits from the neighbouring pentamer in a decamer. The residues from three  $\beta$ -strands ( $\beta$ 2,  $\beta$ 3, and  $\beta$ 4) together with the residues from three  $\alpha$ -helices ( $\alpha$ 2,  $\alpha$ 3 and  $\alpha$ 5) and some residues from the loop connecting  $\alpha$ 2 with  $\beta$ 4 are

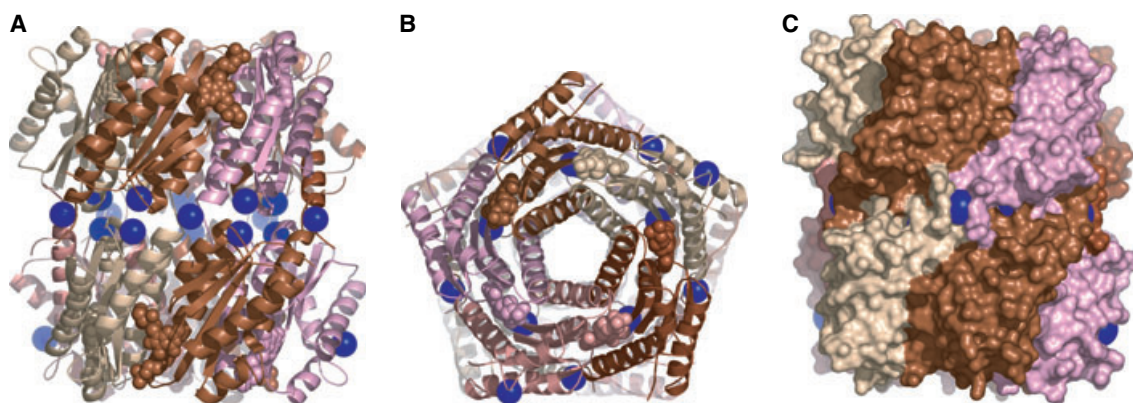


**Fig. 4.** Crystal packing contacts of the pentameric assemblies of lumazine synthase from *M. tuberculosis* viewed perpendicular to the five-fold noncrystallographic axis (A), along the five-fold noncrystallographic axis (B) and surface representation of the assembly viewed perpendicular to the 5-fold noncrystallographic axis (C). The protein subunits belonging to different pentamers are coloured in brown (A- and F-subunits), pink (B- and J-subunits), light brown (C- and I-subunits), light pink (D- and H-subunits) and beige (E- and G-subunits). The active sites, located between subunits, are occupied by 6-(1,3,7-trihydro-9-D-ribityl-2,4,8-purinetrione-7-yl) hexane 1-phosphate (TS68). Blue spheres represent potassium ions. The figure was generated with PYMOL [38].

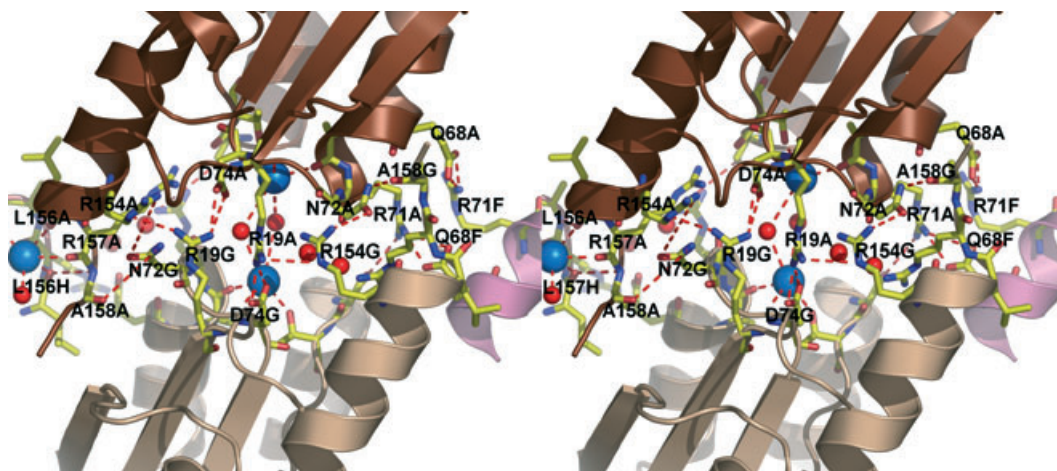


**Fig. 5.** Stereo view of the crystal packing contact area between two pentamers of lumazine synthase from *M. tuberculosis* (A). The protein subunits belonging to different pentamers are coloured in brown (A- and F-subunits), light pink (H-subunit) and beige (G-subunit). The residues involved in the formation of the contacts are shown in ball-and-stick representation and coloured according to the atom type (carbon atoms are yellow, nitrogen atoms are blue and oxygen atoms are red). Blue spheres represent potassium ions, red spheres represent water molecules, and dashed lines represent hydrogen bonds and ionic interactions. The diagram are programmed for cross-eyed (crossed) viewing. The figure was generated with PVMOL [38].

involved in the formation of the contact area. Importantly, almost all interactions have an ionic or polar nature. There are only five residues from 19 with hydrophobic character: Pro51, Val53, Leu69, Leu156 and Ala158. Whereas four arginines (Arg19, Arg71, Arg154 and Arg157), two histidines (His73 and His159), two aspartates (Asp50 and Asp74) and Glu68 form ionic interactions with symmetrical residues of the other pentamer, the residues Val53, Asn72, Ser109 and Ser160 form several direct and water-mediated hydrogen bonds with the respective residues from the other pentamer. Two well-defined salt bridges are formed between Glu68 and Arg71 (subunit A) with the respective Arg71' and Glu68' of another subunit (subunit F), Arg19 and Asp74 from subunit A make two salt-bridges with the respective Asp74' and Arg19' from subunit G. Arg19 is connected by a hydrogen bond to Gly17'N of subunit G, Thr52 is H-bonded to Ala158'O and Arg154' of subunit H, Asn72O<sup>δ1</sup> forms H-bonds to Arg154' and, respectively, Ala158N', Ser109O<sup>γ</sup> makes a hydrogen bond to Arg71', Ser160O<sup>γ</sup> is H-bonded to Val53O (Fig. 5a). One set of potassium ions located in the interface consists of 10 ions coordinated by the residues Ala70, His73, Thr110 of one subunit and usually by three water molecules. The other set of potassium ions is composed of five ions coordinated by four oxygen atoms of the main chain of two different subunits and two water molecules. The distances between potassium atoms and protein atoms are included in Table 2. In C2 crystals, those subunits

**Table 2.** Distances between potassium (K) ions and atoms of lumazine synthase from *M. tuberculosis* residues, involved in ionic interactions in the packing contact area between two pentamers.

Atoms of <i>M. tuberculosis</i> lumazine synthase and water molecules, distances (Å)	Potassium ion	
	K1	K2
OAla70	2.6	
OHis73	2.7	
O <sup>γ</sup> Thr110	2.8	
Wat1	2.7	
Wat2	2.7	
Wat3	2.8	
OLeu156		2.9
OArg157		3.0
OLeu156'		2.8
OArg157'		2.9
Wat4	2.6	
Wat4'		2.6

are related by a crystallographic two-fold axis. The coordination of those potassium ions is also described in detail in [13].

### Binding mode of the purinetriene inhibitors

The inhibitor compounds based on the aromatic purinetriene ring system showed high affinity and specificity to LS from *M. tuberculosis* [22,24]. The structures of the MbtLS complexes with two compounds bearing

the shortest alkyl chains (C3 or C4) were solved and described in detail in our earlier paper [13]. Here we report the structures of MbtLS complexes with four different compounds from the purinetrione series. The electron density maps of the active site regions of those structures are presented in Fig. 6A–D. The binding mode of the heteroaromatic purinetrione system and the additional ribityl chain is similar to that described earlier for the compounds TS44 and TS70 [13]. It is similar to the binding modes of other inhibitors, developed for different LSs [16–18,20,21]. The contacts formed by the MbtLS subunits with each respective inhibitor molecule are listed in Table 3. Generally, the ribityl chain is embedded in the surface depression formed by strand  $\beta 3$  of one subunit and strand  $\beta 5$  of the adjacent subunit. The interaction between two subunits in this interface is formed by two ionic contacts between Glu68 and Arg103 of one subunit and Arg157' and Asp107', respectively, from the neighbouring subunit and by three hydrogen bonds formed between Gln67 and Glu86 of one subunit and Ser109', Leu106' and Gln124' of the adjacent subunit. The ribityl chain positioned in this area is involved in the formation of hydrogen bonds between oxygen atoms of its hydroxyl groups with the main chain nitrogen and main and side-chain oxygen atoms of Ala59 and Glu61 of one subunit and with the main chain nitrogen of Asn114' of the other subunit. The contacts of the ribityl chain to His89 and Lys138' are mediated by a net of water molecules present in the active site cavity. The heteroaromatic purinetrione ring is located in a hydrophobic pocket of the active site formed by the residues Trp27, Ala59, Ile60, Val82 and Val93, and adopts a stacking position with the indole ring of Trp27. It is interesting to note that the side chain of Trp27 was found in either of two different conformations, related by a rotation of 180°. In the MbtLS/TS13 structure (Figs 2 and 6A) the parallel geometry of this interaction is slightly perturbed compared with the other known structures described below, probably due to the absence of the aliphatic chain bearing the phosphate moiety. Whereas the inhibitor TS13 is composed of the purinetrione system and the ribityl chain only, and is lacking the alkyl phosphate chain, the putative position of the second substrate is occupied by a phosphate ion. In all previously described LS structures with a phosphate/sulfate ion located in the position of the second substrate, the phosphate ion formed a strong interaction with the positively charged arginine or histidine residue in the active site.

In the MbtLS/TS13 complex structure, the position of the phosphate ion is found to be shifted from the

Arg128 guanidino group towards the Thr87 hydroxyl group. The size of this shift is slightly different in the different subunits and results in somewhat different lengths of the hydrogen bonds formed by the phosphate ion with the protein residues. This effect can be explained by the existence of the negatively charged Glu136 side chain in close proximity to Arg128 and Lys138. The oxygen atoms of the Glu136 carboxyl group are 3.8 Å apart from Arg128N<sup>e</sup> and 4 Å from Lys138N<sup>ζ</sup>, respectively. The Glu136O<sup>e1</sup> forms a hydrogen bond with N<sup>e2</sup> from Gln141. The water molecule, present in all known MbtLS structures, is linked by hydrogen bonds to the O<sup>e2</sup> of Glu136 with a distance of 2.6 Å and to Glu136O<sup>e1</sup> with a distance of 3.3 Å. The phosphate ion is located at a distance of 3.9 Å from this water molecule. It forms three hydrogen bonds with the atoms O, N and O<sup>γ</sup> of Thr87, with distances of 3.0, 2.6 and 2.5 Å, respectively; a hydrogen bond with the main chain nitrogen atom of Gln86 with a distance of 2.7 Å; and two ionic contacts with N<sup>e</sup> and N<sup>η2</sup> of Arg128 with slightly longer distances of 3.1 and 3.3 Å, respectively.

The phosphate moiety of the compounds TS50, TS51 and TS68 (Figs 2 and 6B–D) occupies almost the same position as the phosphate ion bound in the empty active site and forms the same contacts as a free phosphate. However, the position of the phosphate moiety is shifted towards to the guanidinium group of arginine by shortening of the distance from 3.2 to 3.5 Å to 2.7–2.8 Å. With respect to the length of the aliphatic chain bearing the phosphate group, those contacts can be made directly to the protein atoms or mediated by water molecules. The comparison of MbtLS complexes with purinetrione compounds with an alkyl chain of different length showed that the shift of the phosphate moiety from the aromatic purinetrione system to the periphery of the active site is restricted by the position of Arg128 from one side and the conformation of the loop connecting  $\beta 4$  with  $\alpha 3$  (residues 85–88) from the other side. In the MbtLS/TS44 complex (PDB code 1W19), the phosphorus atom of the phosphate group of TS44 (three carbon atoms) is located at a distance of 5.6 Å from the N4 nitrogen atom of the purine ring. In the complexes of MbtLS with TS70 (PDB code 1W29) (four carbon atoms) and with TS50 (five carbon atoms; Figs 2 and 6B) the phosphate groups are overlapping and found at a distance from N7 of 7.2 Å. In the compound TS51 (five carbon atoms, containing a phosphonate group PO3 instead of phosphate PO4; Figs 2 and 6C), the substitution of the oxygen atom O27 in the phosphate group with the difluoro-methylene group has resulted in a slightly shorter distance

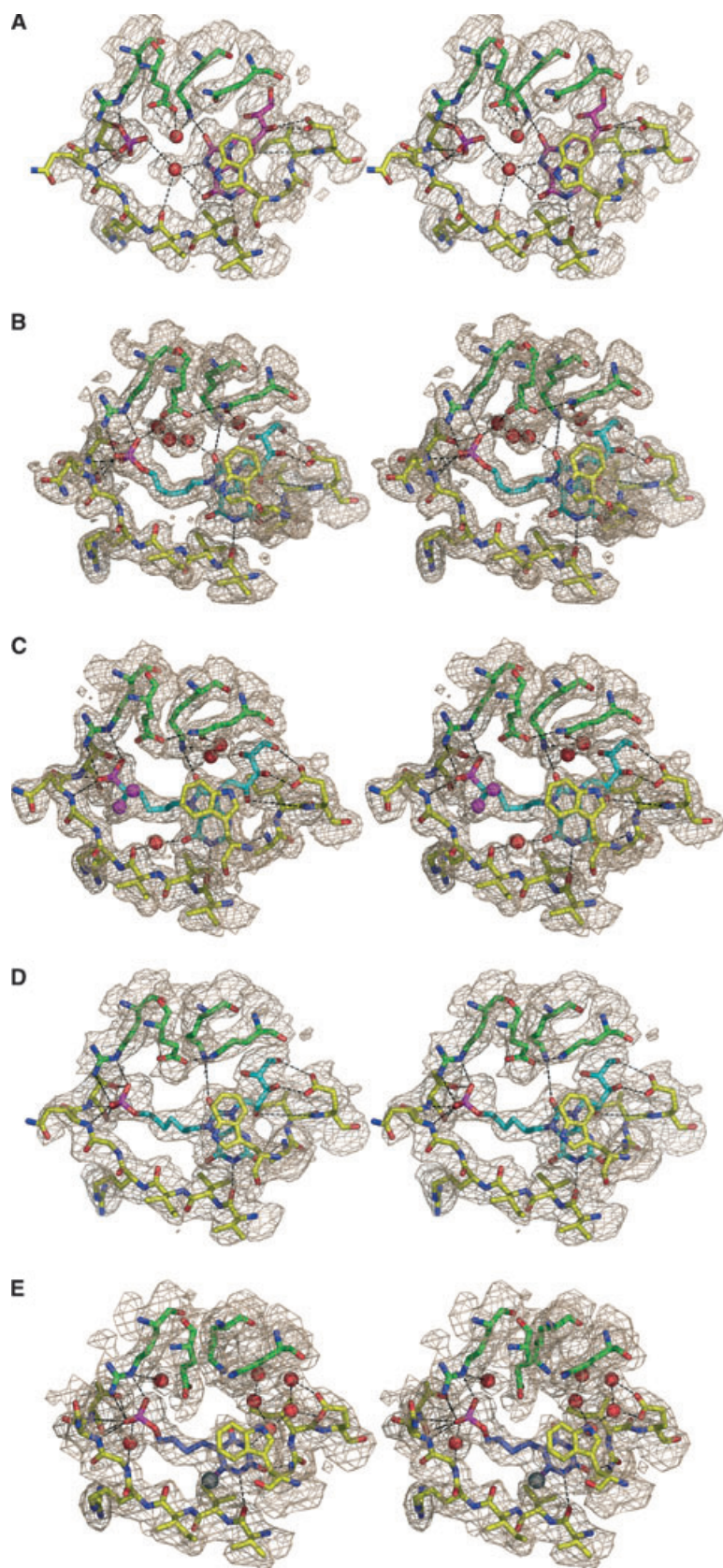


**Fig. 6.** Stereodiagrams of the 2Fol-IFcl electron density map ( $\sigma = 2.5$ ) in the active site region of *M. tuberculosis* lumazine synthase in complex with 1,3,7-trihydro-9-D-ribose-2,4,8-purinetrione (TS13, magenta) (A), 5-(1,3,7-trihydro-9-D-ribose-2,4,8-purinetrione-7-yl) pentane 1-phosphate (TS50, cyan) (B), 5-(1,3,7-trihydro-9-D-ribose-2,4,8-purinetrione-7-yl)1,1-difluoropentane 1-phosphate (TS51, cyan) (C), 6-(1,3,7-trihydro-9-D-ribose-2,4,8-purinetrione-7-yl)hexane 1-phosphate (TS68, cyan) (D) and [4-(6-chloro-2,4-dioxo-1,2,3,4-tetrahydropyrimidine-5-yl)butyl]1-phosphate (JC33, blue) (E). Only the carbon atoms in inhibitors are depicted in the colours states. Red spheres indicate water molecules, dashed lines indicate hydrogen bonds and ionic interactions. The carbon atoms of the residues of different subunits are shown in green and in yellow. The phosphorus atoms are shown in dark pink, fluorine atoms are shown in magenta and the chlorine atom is shown in grey. The diagrams are programmed for cross-eyed (crossed) viewing.

**Table 3.** Distances between inhibitor molecules and atoms of *M. tuberculosis* lumazine synthase, involved in intermolecular H-bonds, ionic and hydrophobic interactions. Distances within 3.5 Å are listed for H-bonds and ionic contacts; distances within 4.5 Å are listed for hydrophobic interactions. (–) Atom does not exist or distance longer than 4 or 5 Å.

Protein atom	Inhibitor atom	MbtLS/TS13 (Å) <sup>a</sup>	MbtLS/TS50 (Å)	MbtLS/TS51 (Å)	MbtLS/TS68 (Å)	MbtLS/JC33 (Å)
NAsn114	O26	2.84	2.86	2.85	3.05	–
OAsn114	O23	3.16	2.81	2.89	3.42	–
O <sup>ε2</sup> Glu61	O26	3.03	2.55	2.70	3.35	–
O <sup>ε2</sup> Glu61	O21	2.89	2.61	2.47	2.76	–
Nlle60	O19	3.48	3.05	3.28	3.50	–
O <sup>γ</sup> Ser25	O2	4.09	2.99	3.18	3.35	–
NAla59	N1	3.88	3.24	2.95	2.96	2.80
OVal81	N3	2.86	2.72	2.80	3.25	3.11
Nlle83	N7	2.73	3.74	3.52	3.45	–
N <sup>ε</sup> Lys138	O8	2.51	2.78	4.01	3.80	–
NGln86	O32(PO <sub>4</sub> )	[2.78]	2.81	3.34	3.12	2.81
NThr87	O33(PO <sub>4</sub> )	[3.11]	2.87	2.81	2.83	3.28
O <sup>γ</sup> Thr87	O33(PO <sub>4</sub> )	[2.48]	2.63	2.62	2.59	2.67
NGly85	F2	–	–	3.05	–	–
N <sup>ε</sup> Arg128	O31(PO <sub>4</sub> )	[2.72]	2.96	2.96	3.07	2.80
N <sup>η2</sup> Arg128	O32(PO <sub>4</sub> )	[2.88]	2.79	3.18	2.85	3.16
Nlle83	Cl	–	–	–	–	3.00
N <sup>ε2</sup> His28	Cl	–	–	–	–	2.96
C <sup>β</sup> Trp27	C2	3.5	3.35	3.37	3.64	3.85
C <sup>β</sup> Ala59	C2	3.84	3.91	4.03	3.86	4.16
C <sup>β</sup> Ile60	C20	4.07	3.84	3.89	4.12	–
C <sup>α</sup> Val82	C4	4.09	3.88	3.95	3.93	–
C <sup>γ1</sup> Val93	C1	4.39	4.33	4.26	–	4.16

<sup>a</sup>The distances between phosphate ion (PO<sub>4</sub><sup>3-</sup>) and protein molecule in MbtLS/TS13 complex are presented in brackets.

between N7 and P atoms, 6.8 Å, whereas the PO<sub>3</sub><sup>-</sup> group clearly strives to occupy the same position. One of the fluorine atoms, F2, forms an additional contact with the hydrogen attached to the nitrogen atom of the main chain (Gly85N). The compound TS68 has the longest aliphatic chain, consisting of six carbon atoms (Figs 2 and 6D). Interestingly, the position of the phosphate group is shifted by only 0.2 Å in comparison with the position of the phosphate group in the MbtLS/TS50, -TS70 and -TS51 complexes. The flexibility of the carbon chain allows for the adoption of different conformations in order to be packed properly in the active site cavity. Apparently, the binding of the phosphate moiety is an energetically more favourable event than any of the conformational changes either in the protein or in the inhibitor molecule. Thus, it can be concluded that the optimal length of the alkyl phosphate chain in the ‘intermediate analogue inhibitors’ is composed of 4–5 carbon atoms. This result is in agreement with the putative structures of the intermediates assumed in the reaction mechanism suggested by Zhang *et al.* [25]. Another important observation, made in line with the first one, was that one or two water mole-

cules were exclusively found in the MbtLS/TS13 structure in the area occupied by the aliphatic chain in the other complexes. Those water molecules form the hydrogen bond network connecting the phosphate ion with the N7 atom of the aromatic purinetrione ring system.

### Binding mode of the chloropyrimidine inhibitor

Compound JC33 ([4-(6-chloro-2,4-dioxo-1,2,3,4-tetrahydropyrimidine-5-yl)butyl]1-phosphate) consists of the C4 alkyl chain bearing the phosphate group and the aromatic pyrimidine ring with the ribityl chain substituted by a chlorine atom (Figs 2 and 6E). This is the first compound among the long list of all known LS inhibitors which does not contain the ribityl chain. The pyrimidinedione ring is ‘flipped over’ relative to its orientation in the other complexes, and the chlorine atom does not simply occupy the space corresponding to the proximal carbon if the ribityl chain in the other structures. The distance between the pyrimidine ring and the phosphate atom in the phosphate moiety is 6.9 Å. The location of this group is the same as in the structures of MbtLS/TS70 and MbtLS/TS50, although

the conformation of the alkyl chain differs from those found in the purinetriene complexes. The phosphate group forms the same contacts as described above for the other inhibitors. The centre of the pyrimidine moiety is located in a position which corresponds to the position of the common bond between the two rings in the purinetriene system (Fig. 3) in complexes of MbtLS with purinetriene derivatives. Previously, the structures of lumazine synthases from *A. aeolicus* and *S. cerevisiae* were solved in complex with another pyrimidine inhibitor (5-(6-D-ribityl-amino-2,4(1*H*,3*H*)pyrimidinedione-5-yl)pentyl 1-phosphonic acid (RPP)) (pdb code 1NQW and 1EJB, respectively) [12,25]. The structural alignment of both structures with the MbtLS/JC33 structure showed a small ( $\sim 1$  Å), shift in the position of the pyrimidine ring, whereas the phosphate and phosphonate moieties occupy the same position in spite of the different conformation of the alkyl chain. The positions of the four hydroxyl oxygen atoms of the ribityl chain are occupied by four water molecules in the MbtLS/JC33 complex. The distance between oxygen atom O2 of the pyrimidine ring and the N<sup>ε</sup> atom of Lys138 is 5.1 Å, and is too long to form a contact found in complexes with purinetriene compounds. Furthermore, the position of O2 is shifted from Lys138'. The stacking interaction between the aromatic pyrimidine ring and the indole group of Trp27 should be weaker in comparison with the purinetriene inhibitors due to the smaller size of the pyrimidine ring. It has in addition resulted in the slight deviation from their parallel ring positions. The shifted position of the pyrimidine system, together with the small size of this group causes different interactions of the carbonyl oxygen atoms of the pyrimidine ring and the protein chain. Namely, there are two new direct hydrogen bonds formed between carbonyl oxygen O1 and the main chain Ala59N and between N1 and Val81O. Four other hydrogen bonds, found in the structures of MbtLS with the purinetriene compounds, are mediated by water molecules in the structure of the MbtLS/JC33 complex. The chlorine atom is involved in two additional contacts with the main chain nitrogen of Ile83 and N<sup>ε2</sup> of His28. In addition to the MPD molecule in the channel, a second MPD molecule was found in the structure of MbtLS/JC33. The molecule is located in the same surface depression as the inhibitor molecule, but  $\sim 10$  Å deeper towards the channel. The position is formed by the residues 112–117 of strand  $\beta 5$  and residues 95–100 of helix  $\alpha 4$  from one subunit and residues 95'–100' from the five-fold symmetry related subunit. The carbonyl oxygen O2 of MPD forms one hydrogen bond with atom O<sup>γ</sup> of Thr98 with a distance of 2.6 Å.

### Isothermal titration calorimetry

In order to determine affinities of the inhibitors described above, isothermal titration calorimetry experiments were carried out using 50 mM potassium phosphate at pH 7. The measurement of the heat released upon binding of the inhibitor allowed us to derive the binding enthalpy of the processes ( $\Delta H$ ), to estimate the stoichiometry ( $n$ ) and association constants ( $K_a$ ), to calculate the entropy ( $\Delta S$ ) and free energy ( $\Delta G$ ) of the binding reactions. Figure 7 shows representative calorimetric titration curves of MbtLS with different inhibitors. Earlier crystallographic studies of lumazine synthases from various organisms (*B. subtilis*, *S. pombe* and *A. aeolicus* [11,25,27]) showed fixed orthophosphate ions bound at the putative site which accepts the phosphate moiety of 3,4-dihydroxy-2-butanone 4-phosphate. The binding of an orthophosphate ion has been recognized as an important feature contributing to the stability of the pentameric assembly in the icosahedral *B. subtilis* enzyme [28]. Thus, the binding free energies and association constants which we have derived from ITC measurements should be considered as 'apparent' free energies and constants, because we are, in fact, dealing with a ternary binding reaction, involving a phosphate ion, an inhibitor molecule and the free enzyme. In line with that finding, enzyme kinetic studies indicated that orthophosphate competes with binding of the substrate, 3,4-dihydroxy-2-butanone 4-phosphate, and with the binding of phosphate-substituted substrate analogues [24]. During the inhibition reaction, this phosphate ion is replaced in competitive manner by the phosphonate or phosphate group of the inhibitor molecule. Thus, neglecting replacement of water molecules, we have measured the binding free energy of the inhibitor reduced by the free energy contribution of phosphate binding at its binding place near Arg128 and Thr87. Due to the fact that all ITC measurements were performed under the same conditions, these apparent values can be used for comparison of binding affinities of the inhibitors under study.

The fitting of the binding isotherms of all five compounds with a binding model assuming identical and independent binding sites gave satisfactory results in contrast to the binding curves of the compounds TS44 and TS70 [13], where good fits were achieved only with the sequential model. The thermodynamic characteristics are shown in Table 4. The binding of all five inhibitors is exothermic with negative changes in the binding enthalpy, similar to the complexes of MbtLS with TS44/TS70 as shown earlier [13]. The association constants are in a range between  $6.54 \times 10^6 \text{ M}^{-1}$  for

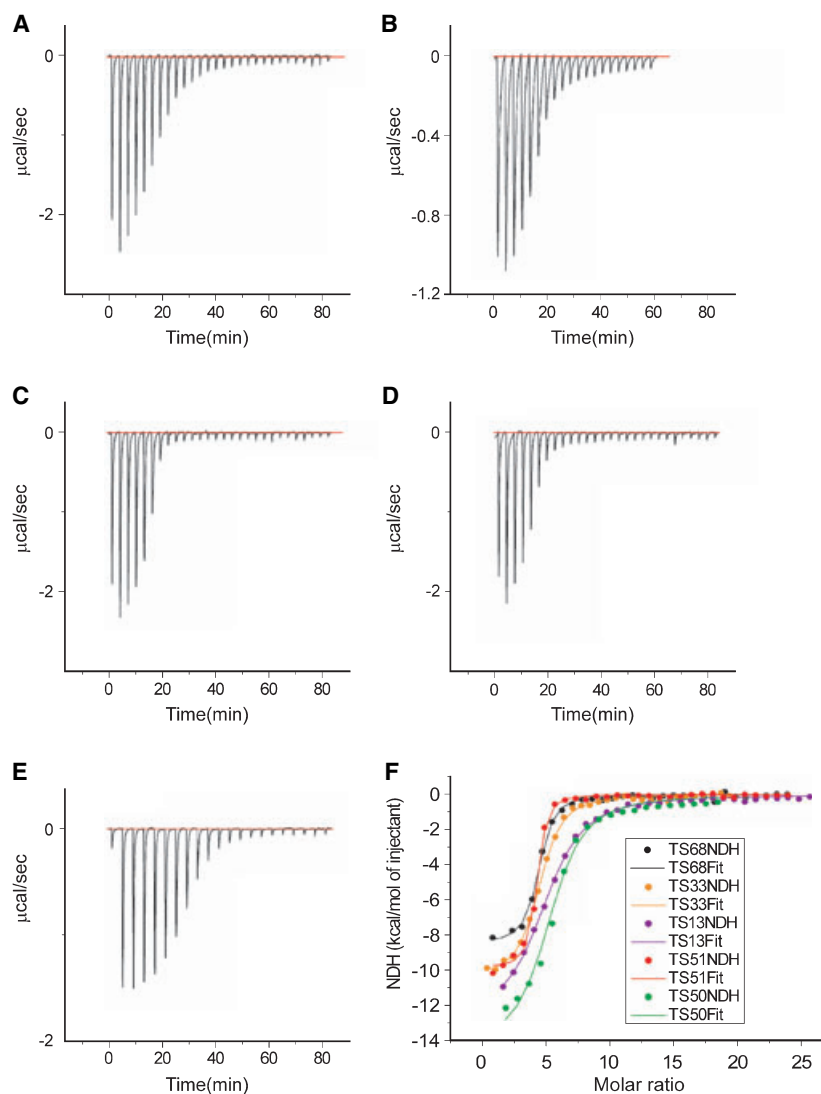


**Fig. 7.** Isothermal titration calorimetry data for lumazine synthase from *M. tuberculosis* titrated with 1,3,7-trihydro-9-D-ribityl-2,4,8-purinetrione (TS13) (A), 5-(1,3,7-trihydro-9-D-ribityl-2,4,8-purinetrione-7-yl)pentane 1-phosphate (TS50) (B), 5-(1,3,7-trihydro-9-D-ribityl-2,4,8-purinetrione-7-yl)1,1-difluoropentane 1-phosphate (TS51) (C), 6-(1,3,7-trihydro-9-D-ribityl-2,4,8-purinetrione-7-yl)hexane 1-phosphate (TS68) (D) and [4-(6-chloro-2,4-dioxo-1,2,3,4-tetrahydropyrimidine-5-yl)butyl]1-phosphate (JC33) (E), and binding isotherms for the inhibitors (F). The filled circles in the binding isotherms represent the experimental values of the heat change at each injection; the continuous lines represent the results of the data fitting to the chosen binding model assuming identical and independent binding sites. The experiments were carried out as described in Experimental procedures.

the MbtLS/TS51 complex and  $3.475 \times 10^5 \text{ M}^{-1}$  for the MbtLS/TS13 complex with corresponding favourable negative binding enthalpy values from  $-8.4 \text{ kcal}\cdot\text{mol}^{-1}$  for MbtLS/TS68 to  $-15.14 \text{ kcal}\cdot\text{mol}^{-1}$  for MbtLS/TS50. The analysis of the thermodynamic parameters of the different inhibitors clearly showed an increase of the affinity (decreasing of  $\Delta G$ ) of the compounds bearing the alkyl phosphate chain in comparison with the phosphate free compound TS13. This observation is in good agreement with the results of the measurements of the inhibition constants by a kinetic inhibition assay described in [24]. Compound TS50 containing a C5-aliphatic chain demonstrated a similar affinity to that described for the compounds TS44 and TS70 previously [13]. The slightly higher affinity which resulted in the larger association constant was obtained for the  $\alpha,\alpha$ -difluorophosphonate compound TS51 and could be explained by the formation of an additional contact

between the fluorine atom F2 and the main chain nitrogen atom of Gly85. Interestingly, a rather large association constant was observed for the complex formation of MbtLS with TS68 (C6). This binding reaction was found to be driven by the least favourable enthalpy change ( $\Delta H = -8.4 \text{ kcal}\cdot\text{mol}^{-1}$ ) among the investigated complexes. The unfavourable change in enthalpy was almost compensated by a corresponding favourable positive change in entropy resulting in a very small free energy change. The observed effect of enthalpy–entropy compensation can be explained by the conformational changes of the aliphatic chain needed for the proper packing of the compound with the longest chain. Those conformational changes are probably responsible for the unfavourable enthalpy changes. The compensating positive entropy term might be due to the rearrangement of the water molecule network in the active site. The molar binding stoichiom-

**Table 4.** Association constants and thermodynamic parameters of binding of different inhibitors to lumazine synthase from *M. tuberculosis*.

	MbtLS/TS13	MbtLS/TS50	MbtLS/TS51	MbtLS/TS68	MbtLS/JC33
Number of sites per pentamer, $n$	4.88 ± 0.06	5.05 ± 0.01	4.86 ± 0.02	4.10 ± 0.01	4.94 ± 0.04
Association constant $K_a$ ( $M^{-1}$ )	347 000 ± 21 600	474 900 ± 91 180	6 540 000 ± 792 100	2 070 000 ± 238 100	1 380 000 ± 103 400
Binding enthalpy $\Delta H$ ( $kcal\cdot mol^{-1}$ )	- 12.87 ± 0.22	- 15.14 ± 0.55	- 9.83 ± 0.09	- 8.46 ± 0.12	- 10.52 ± 0.11
Binding entropy $\Delta S$ ( $cal\cdot mol^{-1}$ ) <sup>a</sup>	- 17.12 ± 0.01	- 23.97 ± 0.02	- 1.26 ± 0.01	0.97 ± 0.01	- 6.61 ± 0.01
Free energy of binding $\Delta G$ ( $kcal\cdot mol^{-1}$ ) <sup>a</sup>	- 7.68 ± 0.04	- 7.88 ± 0.11	- 9.45 ± 0.07	- 8.76 ± 0.07	- 8.52 ± 0.05

<sup>a</sup>The entropy of the binding reactions ( $\Delta S$ ) and the free energy change ( $\Delta G$ ) are obtained from the relation  $\Delta G = -RT \ln(K_a) = \Delta H - T\Delta S$ ; the estimated errors of  $\Delta S$  and  $\Delta G$  are obtained from the relations:  $\sigma_{\Delta G} = \frac{R \cdot T}{K_a} \cdot \sigma_{K_a}$  and  $\sigma_{\Delta S} = \sqrt{\left(\frac{d\Delta S}{d\Delta G} \cdot \sigma_{\Delta G}\right)^2 + \left(\frac{d\Delta S}{dT} \cdot \sigma_{\Delta H}\right)^2} = \sqrt{\left(\frac{1}{T} \cdot \sigma_{\Delta G}\right)^2 + \left(\frac{1}{T} \cdot \sigma_{\Delta H}\right)^2} = \frac{1}{T} \sqrt{\sigma_{\Delta G}^2 + \sigma_{\Delta H}^2}$ , respectively [37].

etry was found to be five bound ligand molecules per pentamer in all five complexes, which is in agreement with the presented X-ray structures. Apparently, the compounds bearing alkyl chains on their C4- and C5-atoms fit better to the active site cavity than the shorter compounds; this is probably due to their ability to form more favourable van der Waals contacts. Conversely, compounds bearing the alkyl phosphate chain need to replace the inorganic phosphate ion and some water molecules in order to be bound to the active site. Those events can be favoured for the compounds with a proper length of the aliphatic chain. In addition, one needs to take into account the fact that the substrate/inhibitor binding site of LS is formed by two neighbouring subunits. The optimal filling of the active site with an inhibitor molecule of proper size, shape and atomic composition clearly stabilizes the interaction of the subunits within the pentamer. This conclusion is in line with all unsuccessful attempts to crystallize LSs from different sources in a substrate/inhibitor-free form. Thus, the dimer with a properly occupied binding site will positively contribute to the stability of the whole pentamer and make the binding of the next inhibitor molecule easier. The five binding sites in the pentamer were found to be structurally identical and the final contacts formed in the complex structures with different inhibitors were found to be rather similar in the different structures. Apparently, the difference of the thermodynamic characteristics observed in the ITC experiments can be explained by weak cooperative behaviour of the binding sites within a pentamer which depends on the specific nature of the inhibitor molecule, particularly depending on the length of the alkyl phosphate chain and the ability of the inhibitor to competitively remove inorganic phosphate. Such weak cooperative behaviour was observed earlier in the MbtLS/TS44 and MbtLS/TS70 binding experiments [13]. However, the JC33 compound containing the C4-alkyl phosphate, which deviates from the purinetrione inhibitors by the presence of a pyrim-

idine ring and the lack of the ribityl chain, showed a medium affinity which was in between the affinity values of TS13 and all the other compounds. The association constant  $K_a$  of JC33 was  $1.38 \times 10^6 M^{-1}$  with a negative enthalpy of  $\Delta H = -10.52 kcal\cdot mol^{-1}$ . This result could be explained by the molecular nature of JC33. According to our structural investigations, this compound lacks four direct contacts with protein atoms made by the hydroxyl groups of the ribityl chain in the other structures. Moreover, several direct contacts with the protein chain by the nitrogen atoms and keto groups of the purinetrione ring system are replaced by contacts formed via water molecules because of the smaller size of the pyrimidine ring. Obviously, the additional contacts formed by the chlorine substituent with His28 and Ile83 (Table 3) are not strong enough to compensate for the interactions made by the purinetrione compounds. In addition, the stacking interaction of the small substituted pyrimidine ring with Trp27 should be generally weaker in comparison with the interaction formed between the purinetrione ring system and the indole system of Trp27. For the bound riboflavin molecule in LS from *S. pombe*, it has been shown that the Trp residue plays an essential role in substrate fixation by  $\pi$ -orbital overlap of the indole ring of Trp with the aromatic rings in the ligand [29]. Thus, the quite high inhibition potential demonstrated by JC33 can rather be explained by the energetically favourable interactions of the phosphate group with Arg128' of one subunit and Gln86, Thr87 from the other subunit.

## Experimental procedures

### Protein expression and purification

*M. tuberculosis* lumazine synthase was obtained by recombinant expression in an *Escherichia coli* strain and purified as reported earlier [13].

## Crystallization

Crystallization trials of MbtLS were performed in the presence of different inhibitors such as 1,3,7-trihydro-9-D-ribityl-2,4,8-purinetrione (TS13), 5-(1,3,7-trihydro-9-D-ribityl-2,4,8-purinetrione-7-yl)pentane1-phosphate (TS50), 6-(1,3,7-trihydro-9-D-ribityl-2,4,8-purinetrione-7-yl)hexane1-phosphate (TS68) 5-(1,3,7-trihydro-9-D-ribityl-2,4,8-purinetrione-7-yl)1,1-difluoropentane-1-phosphate (TS51) and 4-(6-chloro-2,4-dioxo-1,2,3,4-tetrahydropyrimidine-5-yl)butyl 1-phosphate (JC33) (Fig. 2). The crystals were obtained in sitting drops by the vapour diffusion technique with the macroseeding procedure as reported in [13]. The complexes of MbtLS with the inhibitors TS50, TS51 and JC33 were formed in cocrystallization trials and crystallized in the monoclinic space group C2 with slightly different cell dimensions (Table 1). The asymmetric unit contained one pentamer in each case. The data of MbtLS/TS13 and MbtLS/TS68 complexes were evaluated in space group P1 with two pentamers in the crystal cell.

## Data collection

Two X-ray intensity data sets for complexes of MbtLS with TS51 and with JC33 were collected on a MAR Research 345 Image plate detector system (DESY synchrotron beamline BW7B at the EMBL Outstation, Hamburg, Germany) at 100 K each from a single crystal. The optimization of the data collection strategy was performed with the program BEST [30]. Each data set was obtained at a wavelength of 0.85 Å with an oscillation range of 1° per image.

The X-ray data for TS50 bound to MbtLS were collected at 100 K at the synchrotron beamline I7-11 at MAXLAB (Lund, Sweden) with radiation of a wavelength of 1.092 Å and were recorded on a MAR Research 345 Image plate detector.

The X-ray data sets for the complexes of MbtLS with TS13 and TS68 were measured in-house on a MacScience rotating anode generator run at 80mA/40 kV using Cu K $\alpha$  radiation and an OSMIC focusing mirror system. The data were detected on a MAR Research 300 Imaging plate detector system. Both crystals were flash-frozen at 105 K in their respective mother liquor with an Oxford Cryostream cooling device.

Space group and cell parameters for all five data sets were determined using the auto-indexing routine in DENZO [31] and have been checked with pseudo precession images generated with the program PATTERN [32]. The X-ray data were evaluated and scaled with the programs DENZO and SCALEPACK [31]. Statistics of the data collection are given in Table 1. The B-factors calculated from Wilson plots were rather high, namely 67.8 Å<sup>2</sup> and 70.4 Å<sup>2</sup> for MbtLS/TS13 and MbtLS/TS68, respectively, in comparison with the B-factors of the other complexes ( $B_{\text{MbtLS/TS50}} = 22.4 \text{ \AA}^2$ ,  $B_{\text{MbtLS/TS51}} = 25.1 \text{ \AA}^2$ ,  $B_{\text{MbtLS/JC33}} = 31.8 \text{ \AA}^2$ ).

## Structure determination and refinement

The crystal structures of all five complexes were solved by molecular replacement using the programs AMORE and MOLREP as implemented in CCP4 [33]. The pentamer structure of lumazine synthase from the earlier reported MbtLS/TS44 complex [13] (pdb code 1W19), excluding the coordinates for the inhibitor, was successfully used as a search model for each data set.

In each case, the initial pentameric model was firstly subjected to rigid body refinement in CNS [34]. Each of the five (MbtLS complexes with TS50, TS51 and JC33, respectively) or 10 (MbtLS/TS13, MbtLS/TS68 complexes) subunits was considered as a rigid group. The resulting coordinates were used to calculate the initial 2|Fo|-|Fc| and |Fo|-|Fc| electron density maps in order to verify the appearance of the inhibitor molecules. The initial electron density maps were subjected to solvent flattening, histogram matching and five-fold noncrystallographic averaging with the program DM as implemented in the CCP4 package [33]. The mask covering one subunit was calculated with NCSMASK [33]. The noncrystallographic symmetry operators were improved after every five cycles of averaging. The resulting electron density maps of all complexes were well defined and allowed the building of the respective inhibitor molecules. All model building was performed with O [35]. The molecular models for the inhibitors were generated with Monomer Library Sketcher [33]. The dictionaries and libraries needed for the rebuilding and refinement were prepared by HIC-UP [36]. The optimization of the geometric parameters was performed with CNS. Further refinement using the TLS option in order to take into account the thermal displacement of each subunit was carried out with the program REFMAC5 [33]. Protein subunits and later inhibitor molecules were assigned as separate TLS groups. The progress of refinement was monitored by the free R-factor with 5% of the data put aside from the calculations. The five-fold noncrystallographic restraints were not applied for the complexes of MbtLS with TS50, TS51 and JC33, however, tight restraints for the main chain atoms and medium restraints for the side chains were used throughout the refinement for the data sets of MbtLS with TS13 and TS68. After inclusion of the bound inhibitors and subsequent refinement of the protein models, solvent molecules were added with the help of the ARP/WARP program as implemented in the CCP4 package. In addition to MbtLS subunits and inhibitor molecules, potassium ions, dithiothreitol molecules, acetate ions, MPD molecules and some water molecules were built into the |Fo|-|Fc| map manually. Details of the refinement statistics are presented in Table 1. The atomic coordinates and structure factors of MbtLS/TS13, MbtLS/TS50, MbtLS/TS51, MbtLS/TS68 and MbtLS/JC33 complexes have been deposited at Protein Data Bank, accession codes are 2C9B, 2C92, 2C94, 2C9d, and 2C97, respectively,

## Inhibitors

The inhibitors 1,3,7-trihydro-9-D-ribityl-2,4,8-purinetrione (TS13), 5-(1,3,7-trihydro-9-D-ribityl-2,4,8-purinetrione-7-yl)pentane1-phosphate (TS50), 6-(1,3,7-trihydro-9-D-ribityl-2,4,8-purinetrione-7-yl)hexane1-phosphate (TS68), and 5-(1,3,7-trihydro-9-D-ribityl-2,4,8-purinetrione-7-yl)1,1-difluoropentane1-phosphate (TS51) were designed by Cushman *et al.* [24] in order to investigate the most important structural details of the inhibition of lumazine synthase from *M. tuberculosis*. Those compounds contain structural elements corresponding to both of the substrates and can be classified as 'intermediate analogue inhibitors'. 4-(6-Chloro-2,4-dioxo-1,2,3,4-tetrahydropyrimidine-5-yl) butyl1-phosphate (JC33) was synthesized by Cushman *et al.* (M.C., unpublished results).

## Isothermal titration calorimetry

The calorimetric measurements of the binding of each inhibitor were carried out using a VP-ITC MicroCalorimeter (MicroCal, Inc., Northampton, MA, USA) as described earlier [13]. All data were evaluated with the Microcal ORIGIN50 Software package (Microcal Software, INC., Northampton, MA, USA). The association constants,  $K_a$ , binding enthalpy,  $\Delta H$ , and stoichiometry,  $n$ , were obtained by fitting the data to standard equations for the binding using a model for identical independent sites (One Set of Sites model) as implemented in the MICROCAL ORIGIN50 package. The fitting procedure was performed for the reaction scheme  $M + nX = MX_n$  in agreement with the following equations:  $K = \frac{\Theta}{(1-\Theta)[X]}$  and  $X_t = [X] + n\Theta M_t$ , where  $K$  is the binding constant;  $n$ , number of sites;  $M_t$ , total concentration of macromolecule in  $V_0$ ;  $X_t$  and  $[X]$  are total and free concentrations of ligand, and  $\Theta$  is the fraction of sites occupied by ligand  $X$ . The initial estimates for  $n$ ,  $K_a$  and  $\Delta H$  were refined by standard Marquardt nonlinear regression methods. The binding entropy  $\Delta S$  and free energy  $\Delta G$  of the binding process were calculated from the basic thermodynamic equations,  $\Delta G = -RT \ln K$  and the Gibbs-Helmholtz equation  $\Delta G = \Delta H - T\Delta S$ .

## Acknowledgements

We thank Xiaofeng Zhang and Winfried Meining for help with the data collection of the complexes MbtLS/TS51, MbtLS/JC33 and MbtLS/TS50, respectively. We gratefully acknowledge the access to synchrotron radiation facilities at the EMBL Outstation in Hamburg and MAXLab in Lund and thank Alexander Popov for excellent help at the beamline. This work was supported by the Swedish Research Council (Vetenskapsrådet) (Project No. 621-2001-3195), NIH Grant GM 51469, the Hans Fischer Gesellschaft e.V. and the Fonds der Chemischen Industrie.

## References

- 1 Nakajima H (1993) Tuberculosis: a global emergency. *World Health* **46**, 3.
- 2 Cole ST, Brosch R, Parkhill J, Garnier T, Churcher C, Harris D, Gordon SV, Eiglmeier K, Gas SCEB III, Tekaia F, *et al.* (1998) Deciphering the biology of *Mycobacterium tuberculosis* from the complete genome sequence. *Nature* **393**, 537–544.
- 3 Sasseti CM, Boyd DH & Rubin EJ (2003) Genes required for mycobacterial growth defined by high density mutagenesis. *Mol Microbiol* **48**, 77–84.
- 4 Sasseti CM & Rubin EJ (2003) Genetic requirements for mycobacterial survival during infection. *Proc Natl Acad Sci USA* **100**, 12989–12994.
- 5 Bacher A, Baur R, Eggers U, Harders HD, Otto MK & Schnepfle H (1980) Riboflavin synthases of *Bacillus subtilis*. Purification and properties. *J Biol Chem* **255**, 632–637.
- 6 Cushman M, Patel HH, Scheuring J & Bacher A (1992)  $^{19}\text{F}$  NMR studies on the mechanism of riboflavin synthase: synthesis of 6-(trifluoromethyl)-7-oxo-8-(D-ribityl) lumazine and 6-(trifluoromethyl)-7-methyl-8-(D-ribityl) lumazine. *J Org Chem* **57**, 5630–5643.
- 7 Ladenstein R, Schneider M, Huber R, Bartunik HD, Wilson K, Schott K & Bacher A (1988) Heavy riboflavin synthase from *Bacillus subtilis*: crystal structure analysis of the icosahedral  $\beta_{60}$  capsid at 3.3 Å resolution. *J Mol Biol* **203**, 1045–1070.
- 8 Zhang X, Meining W, Fischer M, Bacher A & Ladenstein R (2001) X-ray structure analysis and crystallographic refinement of lumazine synthase from the hyperthermophile *Aquifex aeolicus* at 1.6 Å resolution: determinants of thermostability revealed from structural comparisons. *J Mol Biol* **306**, 1099–1114.
- 9 Persson K, Schneider G, Jordan DB, Viitanen PV & Sandalova T (1999) Crystal structure analysis of a pentameric fungal and an icosahedral plant lumazine synthase reveals the structural basis for differences in assembly. *Protein Sci* **8**, 2355–2365.
- 10 Braden BC, Velikovskiy CA, Cauerhff AA, Polikarpov I & Goldbaum FA (2000) Divergence in macromolecular assembly: X-ray crystallographic structure analysis of lumazine synthase from *Brucella abortus*. *J Mol Biol* **297**, 1031–1036.
- 11 Gerhardt S, Haase I, Steinbacher S, Kaiser JT, Cushman M, Bacher A, Huber R & Fischer M (2002) The structural basis of riboflavin binding to *Schizosaccharomyces pombe* 6,7-dimethyl-8-ribityllumazine synthase. *J Mol Biol* **318**, 1317–1329.
- 12 Meining W, Mörtl S, Fischer M, Cushman M, Bacher A & Ladenstein R (2000) The atomic structure of pentameric lumazine synthase from *Saccharomyces cerevisiae* at 1.85 Å resolution reveals the binding mode of a phosphonate intermediate analogue. *J Mol Biol* **299**, 181–197.

- 13 Morgunova E, Meining W, Cushman M, Illarionov B, Haase I, Jin G, Bacher A, Cushman M, Fischer M & Ladenstein R (2005) Crystal structure of lumazine synthase from *Mycobacterium tuberculosis* as a target for rational drug design: binding mode of a new class of purinetrione inhibitors. *Biochemistry* **44**, 2746–2758.
- 14 Ludwig ML, Pattridge KA, Smith WW, Jensen LH & Watenpaugh KD (1982) *Flavins and Flavoproteins*. Elsevier, Amsterdam.
- 15 Volk R & Bacher A (1991) Biosynthesis of riboflavin. Studies on the mechanism of L-3,4-dihydroxy-2-butanone 4-phosphate synthase. *J Biol Chem* **266**, 20610–20618.
- 16 Cushman M, Mavandadi F, Kugelbrey K & Bacher A (1997) Design and synthesis of (ribitylamino) uracils bearing fluorosulfonyl, sulfonic acid, and carboxylic acid functionality as inhibitors of lumazine synthase. *J Org Chem* **62**, 8944–8947.
- 17 Cushman M, Mavandadi F, Kugelbrey K & Bacher A (1998) Synthesis of 2,6-dioxo-(1*H*,3*H*)-9-*N*-ribityl-purine and 2,6-dioxo-(1*H*,3*H*)-8-aza-9-*N*-ribityl-purine as inhibitors of lumazine synthase and riboflavin synthase. *Bioorg Medical Chem* **6**, 409–415.
- 18 Cushman M, Mavandadi F, Yang D, Kugelbrey K, Kis K & Bacher A (1999) Synthesis and biochemical evaluation of bis (6,7-dimethyl-8-*D*-ribityllumazines) as potential bisubstrate analogue inhibitors of riboflavin synthase. *J Org Chem* **64**, 4635–4642.
- 19 Cushman M, Mihalic JT, Kis K & Bacher A (1999) Design and synthesis of 6-(6-*D*-ribitylamino-2,4-dihydroxypyrimidin-5-yl)-1-hexyl-phosphonic acid, a potent inhibitor of lumazine synthase. *Bioorganic Med Chem Lett* **9**, 39–42.
- 20 Cushman M, Mihalic JT, Kis K & Bacher A (1999) Design, synthesis, and biological evaluation of homologous phosphonic acids and sulfonic acids as inhibitors of lumazine synthase. *J Org Chem* **64**, 3838–3845.
- 21 Cushman M, Yang D, Gerhardt S, Huber R, Fischer M, Kis K & Bacher A (2002) Design, synthesis, and evaluation of 6-carboxyalkyl and 6-phosphonoxyalkyl derivatives of 7-oxo-8-ribitylamino-lumazines as inhibitors of riboflavin synthase and lumazine synthase. *J Org Chem* **67**, 5807–5816.
- 22 Cushman M, Yang D, Kis K & Bacher A (2001) Design, synthesis, and evaluation of 9-*D*-ribityl-1,3,7-trihydro-2,4,8-purinetrione, a potent inhibitor of riboflavin synthase and lumazine synthase. *J Org Chem* **66**, 8320–8327.
- 23 Ladenstein R, Ritsert K, Huber R, Richter G & Bacher A (1994) The lumazine synthase/riboflavin synthase complex of *Bacillus subtilis*: X-ray structure analysis of hollow reconstituted  $\beta$ -subunit capsids. *Eur J Biochem* **223**, 1007–1017.
- 24 Cushman M, Sambaiah T, Jin G, Illarionov B, Fischer M & Bacher A (2004) Design, synthesis, and evaluation of 9-*D*-ribitylamino-1,3,7,9-tetrahydro-2,6,8-purine-triones bearing alkyl phosphate and alpha, alpha-difluorophosphonate substituents as inhibitors of riboflavin synthase and lumazine synthase. *J Org Chem* **69**, 601–612.
- 25 Zhang X, Meining W, Cushman M, Haase I, Fischer M, Bacher A & Ladenstein R (2003) A structure-based model of the reaction catalyzed by lumazine synthase from *Aquifex aeolicus*. *J Mol Biol* **328**, 167–182.
- 26 Klinke S, Zylberman V, Vega DR, Guimaraes BG, Braden BC & Goldbaum FA (2005) Crystallographic studies on decameric *Brucella* spp. lumazine synthase: a novel quaternary arrangement evolved for a new function? *J Mol Biol* **353**, 124–137.
- 27 Schott K, Ladenstein R, Konig A & Bacher A (1990) The lumazine synthase-riboflavin synthase complex of *Bacillus subtilis*: crystallization of reconstituted icosahedral  $\beta$ -subunit capsids [published erratum appears in *J Biol Chem* 1990 **15**, 18041]. *J Biol Chem* **265**, 12686–12689.
- 28 Bacher A, Ludwig HC, Schnepfle H & Ben-Shaul Y (1986) Heavy riboflavin synthase from *Bacillus subtilis*: quaternary structure and reaggregation. *J Mol Biol* **187**, 75–86.
- 29 Michael Koch CB, Gerhardt S, Haase I, Weber S, Cushman M, Huber R, Bacher A, Fischer M (2004) Structural basis of charge transfer complex formation by riboflavin bound to 6,7-dimethyl-8-ribityllumazine synthase. *Eur J Biochem* **271**, 3208–3214.
- 30 Bourenkov GP & Popov AN (2006) A quantitative approach to data-collection strategies. *Acta Crystallogr D Biol Crystallogr* **62**, 58–64.
- 31 Otwinowski Z & Minor W (1997) Processing of X-ray diffraction data collected in oscillation mode. *Methods Enzymol* **276**, 307–326.
- 32 Lu G (1999) PATTERN: a precession simulating program for displaying reflection data of reciprocal space. *J Appl Crystallogr* **32**, 375–376.
- 33 Collaborative Computational Project N (1994) The CCP4 Suite: programs for protein crystallography. *Acta Cryst* **D50**, 760–763.
- 34 Brünger AT, Adams PD, Clore GM, DeLano WL, Gros P, Grosse-Kunstleve RW, Jiang J-S, Kuszewski J, Nilges M, Pannu NS, *et al.* (1998) Crystallography & NMR System: a new software suite for macromolecular structure determination. *Acta Cryst* **D54**, 905–921.
- 35 Jones AT, Zou JY, Cowtan JY & Kjeldgaard M (1991) Improved methods for building protein models in electron density maps and the location of errors in the model. *Acta Crystallogr* **A47**, 110–119.
- 36 Kleywegt GJ & Jones TA (1998) Databases in protein crystallography. *Acta Cryst* **D54**, 1119–1131.
- 37 Taylor JR (1997) *An Introduction to Error Analysis: the Study of Uncertainties in Physical Measurements*, 2nd edn. edn, University Science Books, Sausalito.
- 38 DeLano WL (2002) The PyMOL Molecular Graphics System. DeLano Scientific, San Carlos, CA, USA.